

# Dalton Transactions

Accepted Manuscript

This article can be cited before page numbers have been issued, to do this please use: J. Feng, C. Ma, P. Miedziak, J. Edwards, G. Brett, D. Li, Y. Du, D. Morgan and G. Hutchings, *Dalton Trans.*, 2013, DOI: 10.1039/C3DT51855H.



This is an *Accepted Manuscript*, which has been through the RSC Publishing peer review process and has been accepted for publication.

*Accepted Manuscripts* are published online shortly after acceptance, which is prior to technical editing, formatting and proof reading. This free service from RSC Publishing allows authors to make their results available to the community, in citable form, before publication of the edited article. This *Accepted Manuscript* will be replaced by the edited and formatted *Advance Article* as soon as this is available.

To cite this manuscript please use its permanent Digital Object Identifier (DOI®), which is identical for all formats of publication.

More information about *Accepted Manuscripts* can be found in the [Information for Authors](#).

Please note that technical editing may introduce minor changes to the text and/or graphics contained in the manuscript submitted by the author(s) which may alter content, and that the standard [Terms & Conditions](#) and the [ethical guidelines](#) that apply to the journal are still applicable. In no event shall the RSC be held responsible for any errors or omissions in these *Accepted Manuscript* manuscripts or any consequences arising from the use of any information contained in them.

absence of acidity can switch-off the disproportionation reaction of benzyl alcohol and thus exhibit much higher selectivity to the aldehyde; however, this desirable selectivity was accompanied by low benzyl alcohol conversion.<sup>32</sup> Hence, developing new types of metal catalyst that can exhibit controllable surface acidic or basic properties of supports could be of value. Layered double hydroxide (LDH), known as a family of synthetic anionic clays, are a class of two-dimensional brucite  $Mg(OH)_2$ -like layered inorganic materials. They can be expressed by the general formula  $[M^{2+}_{1-x}M^{3+}_x(OH)_2]^{x+}(A^{n-})_{x/n} \cdot mH_2O$ .<sup>33</sup> As a consequence of the tailored structure-design and controlled accessibility to catalytic sites, LDH provide potential opportunities for designing and innovating novel catalyst supports, catalyst precursors as well as actual catalysts.<sup>34-36</sup> In particular, calcination of LDHs at intermediate temperatures (450-600 °C) often gives poorly crystallized mixed metal oxides (MMO), which possess higher surface area and tunable surface acidic/basic properties.<sup>37</sup> Knowing that MgAl-MMO has both strong acid and base sites on their surfaces, herein, we report the research on the specific combination of bimetallic Au-Pd nanoparticles with the acid-base bifunctional material of MgAl-MMO as a novel heterogeneous catalyst for solvent-free oxidation of benzyl alcohol using molecular oxygen. HRTEM, XPS, *In situ* FT-IR of CO and  $NH_3/CO_2$ -TPD were employed to investigate the structure and composition of the catalyst and reveal the synergistic effect between Au and Pd as well as the unique cooperative interaction between the bimetallic Au-Pd and surface acidic/basic sites on the MMO support.

## Experimental

**Support preparation:** MgAl-MMO support was derived from an MgAl-LDH precursor. MgAl-LDH precursor was prepared by means of a hydrothermal synthesis method.  $Mg(NO_3)_2 \cdot 6H_2O$ ,  $Al(NO_3)_3 \cdot 9H_2O$  and urea with an  $Mg^{2+}/Al^{3+}$ /urea molar ratio of 2:1:7 were dissolved in 80 mL deionized water to make a mixed solution. The resulting solution was transferred to an autoclave and aged at 150 °C for 6 h. The precipitate was then centrifuged and thoroughly washed with deionized water until the filtrate reached pH 7. After drying and calcination at 450 °C for 4 h, MgAl-LDH precursor transformed into MgAl-MMO support.

**Catalyst preparation:** Supported Au, Pd and Au-Pd catalysts were prepared using a sol-immobilization method. An aqueous solution of  $PdCl_2$  and  $HAuCl_4 \cdot 3H_2O$  (Johnson Matthey) of the desired concentration was prepared. For the bimetallic catalyst with the Au:Pd molar ratio of 1:1, the detailed preparation procedure employed is described below. To an aqueous  $PdCl_2$  and  $HAuCl_4$  solution of the desired concentration, the required amount of a PVA solution (1 wt %) was added (PVA/(Au+Pd) (wt/wt)=1.2); a freshly prepared solution of  $NaBH_4$  (0.1 M,  $NaBH_4$ /(Au+Pd) (mol/mol)=5) was then added to form a dark-brown sol. After 30 min of sol generation, the colloid was immobilized by adding support under vigorous stirring conditions. The amount of support material required was calculated so as to have a total final metal loading of 1 % wt. After 1 h the slurry was filtered, the catalyst washed thoroughly with distilled water and dried at 120 °C overnight. This sample is denoted as 1% Au-Pd/MgAl-MMO. Other bimetallic catalysts with different molar ratio of Au/Pd were prepared as stated above keeping the total

metal loading of 1% wt.

Monometallic catalysts containing only gold or palladium were prepared using a similar methodology, and these are denoted 1% Au/MgAl-MMO, 1% Pd/MgAl-MMO, 0.65% Au/MgAl-MMO and 0.35% Pd/MgAl-MMO respectively.

**Catalyst characterization:** Powder XRD patterns were recorded on a Shimadzu XRD-600 X-ray powder diffractometer (Cu  $K_\alpha$  radiation,  $\lambda = 0.15406$  nm) between 3° and 70° 2 $\theta$ , with a scan speed of 10 ° min<sup>-1</sup>. Elemental analysis was performed using a Shimadzu ICPS-75000 inductively coupled plasma emission spectrometer (ICP-ES) and an Elementar Vario EL elemental analyzer. The morphology, size distribution, lattice fringe and crystal boundaries of the samples were examined using JEOL J-2100 high-resolution transmission electron microscopy (HRTEM). UV-visible analysis of the colloidal sols was used to monitor the intensity and position of the plasmon resonance band of gold using a Shimadzu UV-2501PC UV-visible spectrophotometer. The low temperature  $N_2$  adsorption-desorption experiments were carried out on a Micromeritics Surface Area & Porosity Gemini VII 2390. XPS measurements were performed on a Kratos Axis Ultra DLD photoelectron spectrometer using monochromatic Al  $K_\alpha$  radiation. The mixed metal oxides were calibrated to the Mg 2p photoelectron peak at 49.6 eV as measured from pure MgO and  $MgAl_2O_4$  samples and consistent with that reported in the literature.<sup>38</sup>

$CO_2$  and  $NH_3$ -TPD of the catalysts were conducted on a Micromeritics ChemiSorb 2720. About 100 mg of samples were loaded in a quartz reactor and heated in He for 60 min at 120 °C, followed by treating with the probe molecules (25 mL/min) for 60 min at room temperature. Weakly adsorbed probe molecules were removed by flowing He for 120 min, and then desorption process was carried out from room temperature to 800 °C in He flow with the rate of 10 °C/min.

*In situ* Fourier-transformed infrared absorption spectroscopy of CO experiments were carried out in a custom built quartz cell equipped with KBr windows allowing sample activation and successive measurements in the range of 292–823 K, at pressures as low as 10<sup>-4</sup>. The catalysts were pressed into self-supporting pellets and activated in the same cell used for the measurement. The thermal treatments were performed either in dynamic vacuum or under static conditions (no flux), according to procedures discussed below. *In situ* FTIR spectra on the investigated catalysts were recorded at a resolution of 0.964 cm<sup>-1</sup> on a Nicolet 380 instrument. After nitrogen pre-treatment at 100 °C for 45 minutes and hydrogenation treatment at 100 °C for 60 minutes, the catalyst was scanned to get a background record below a pressure of 10<sup>-3</sup> Pa. And then the catalyst was exposed to a CO flow for 60 minutes. Sample scanning for adsorbed CO on catalysts was conducted after the pressure was reduced below 10<sup>-3</sup> Pa again.

**Benzyl alcohol oxidation:** Benzyl alcohol oxidation was carried out in a 50 mL glass stirred reactor. In a typical reaction, 10 mg catalyst and 1 mL benzyl alcohol were charged into the reactor which was then purged with  $O_2$  three times before closing and the pressure was maintained at 1 bar (relative pressure). The reactor with the reaction mixture was kept in a heating block, which was preheated to the reaction temperature. The reaction mixture was stirred at 1000 rpm using a magnetic bar inside the

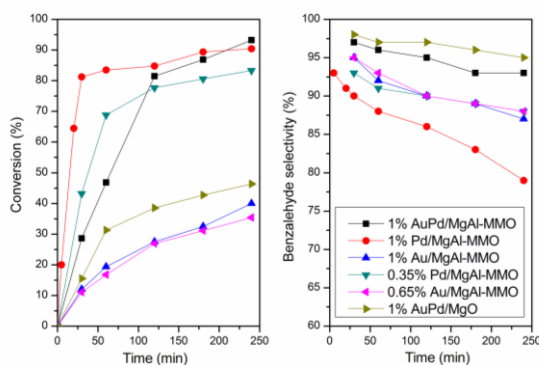
reactor. After a specific time, the stirring was stopped and the reactor was rapidly cooled in an ice bath. After cooling for 10 min, the reactor was opened slowly and the contents were centrifuged.

5 An aliquot of the clear supernatant reaction mixture (0.5 mL) was diluted with mesitylene (0.5 mL, external standard for GC analysis) Samples were removed periodically and analysed by GC. For the analysis of the products a GC-MS (Waters, GCT Premier) and GC (a Varian star 3400 cx with a 30 m CP-Wax 52  
10 CB column) were employed. The products were identified by comparison with known standards. For the quantification of the amounts of reactants consumed and products generated, an external standard method was used. The selectivity was calculated as mol of product formed per mol of reacted benzyl  
15 alcohol and the carbon balance was within  $\pm 5\%$ .

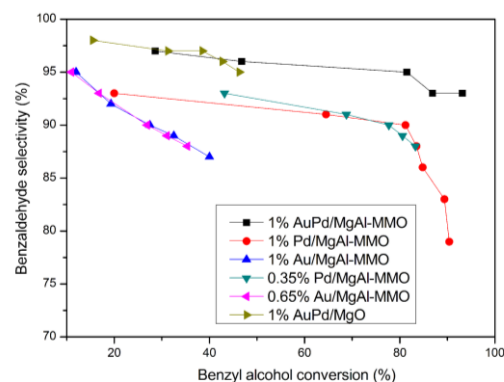
## Result and discussion

### Synergistic effect of Au and Pd

The catalytic oxidation of benzyl alcohol under solvent-free conditions has been investigated at 140 °C with 1 bar oxygen  
20 using a glass reactor and the results are shown in Figure 1. The monometallic Pd/MgAl-MMO catalysts exhibited very high initial activity, but the selectivity to benzaldehyde decreased significantly with the time on line. In the case of 1% Pd/MgAl-MMO, the selectivity to benzaldehyde decreased to <80% after  
25 240 min. As for the Au/MgAl-MMO catalysts, the benzyl alcohol conversions were much lower and the Au loading had little influence on the catalytic activity, indicating the pure Au catalyst is less active for this reaction. In contrast, the bimetallic  
30 AuPd/MgAl-MMO catalyst was both active and selective for this reaction. The conversion of benzyl alcohol reached ca. 93% after 240 min and the selectivity towards benzaldehyde maintained ca. 93%. Furthermore, when expressed in terms of the conversion (Fig. 2) it is possible to compare the selectivities towards  
35 benzaldehyde at iso-conversion (since in oxidation reactions selectivity can be a function of conversion). It is apparent that the bimetallic Au-Pd/MgAl-MMO catalyst gave much higher benzaldehyde selectivity than both pure Pd and Au catalyst at iso-conversion which illustrates a very pronounced synergistic effect between Au and Pd.



40 **Figure 1** Catalytic performance of MgAl-MMO supported 1% Au-Pd, 1% and 0.65% Au, 1% and 0.35% Pd and MgO supported 1% Au-Pd



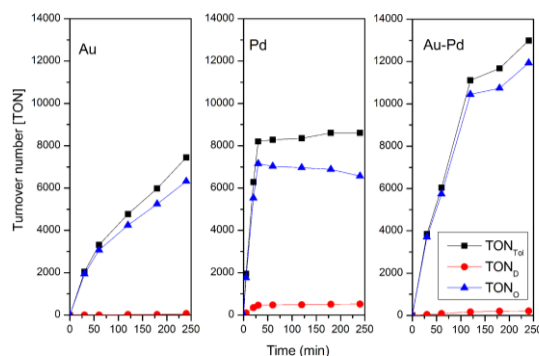
45 **Figure 2** Selectivity to benzaldehyde as a function of benzyl alcohol conversion

As we have previously reported, benzaldehyde, the target product, can be formed by both selective oxidation and  
50 disproportionation of benzyl alcohol.<sup>32</sup> In the present work, we quantify these two reactions separately and try to understand the effect of the nature of the catalyst on these two reactions. The separation and quantification of these two reactions has been performed using the following underlying premise. Benzaldehyde  
55 is formed from the reactions of both oxidation and disproportionation, therefore it cannot be used to quantify either reaction. However, toluene is formed exclusively from disproportionation; therefore the amount of toluene can be used as a measure of the extent of the disproportionation reaction,  
60 since in this reaction equimolar amounts of toluene and benzaldehyde are produced. The turnover numbers for the oxidation reaction ( $TON_O$ ), disproportionation reaction ( $TON_D$ ) and the overall reaction ( $TON_{Tot}$ ) were calculated using the following equations and the results are plotted in Figure 3.

$$TON_D = \frac{2 * mol_{tol}}{mol_{metal}}$$

$$TON_O = \frac{mol_{PhCHO} - mol_{tol}}{mol_{metal}}$$

$$TON_{Tot} = \frac{mol_{PhCHO} + mol_{tol}}{mol_{metal}}$$



70 **Figure 3** Reaction time profiles of the turnover numbers over MgAl-MMO supported 1% Au-Pd, 1% Pd, and 1% Au

It is apparent that the pure Au catalyst was almost inactive for the disproportionation reaction and the  $TON_{Tot}$  was very close to

the  $\text{TON}_0$ , which indicates that the oxidation reaction was the only active reaction over the pure Au catalyst. However, a small increase of  $\text{TON}_D$  was observed over the Pd catalyst after 30 min, while the  $\text{TON}_O$  decreased slightly. This illustrates that the oxidation reaction was suppressed after 30 min and a very slow disproportionation reaction was observed exclusively with the pure Pd catalyst, however, the reaction was largely inhibited after 30 min. After alloying Au with Pd, the  $\text{TON}_D$  remained at a low level, while the  $\text{TON}_{\text{Tot}}$  increased to 13000 after 240 min which was evidently higher than that of the pure Pd (8610) and Au catalyst (7445). These results further confirm the positive synergistic effect of alloying gold and palladium for the selective oxidation of benzyl alcohol.

Besides toluene derived from disproportionation reaction, there are still a number of by-products that can be formed by over-oxidation of benzyl alcohol e.g. benzoic acid, benzyl benzoate, benzene, dibenzylether and dibenzyl acetal.<sup>39</sup> Figure 4 shows the selectivity towards major by-products formed by over-oxidation of benzyl alcohol as a function of benzyl alcohol conversion for the Au, Pd and bimetallic Au-Pd catalysts. In the case of Pd catalyst, the selectivity to benzene, benzoic acid and benzyl benzoate increased significantly with the benzyl alcohol conversion increasing. For the pure Au catalyst, although the selectivity to benzene and benzoic acid maintained in a low level (<1%), the selectivity towards benzyl benzoate dramatically increased to 13% when the benzyl alcohol conversion reached 40%. It is possible that benzaldehyde reacts with benzyl alcohol to form a hemiacetyl and this is oxidised to benzyl benzoate.<sup>18</sup> However, the selectivities to all the three by-products over Au-Pd catalyst were much lower, which demonstrates that alloying Pd with Au could effectively suppress the over-oxidation of benzyl alcohol.

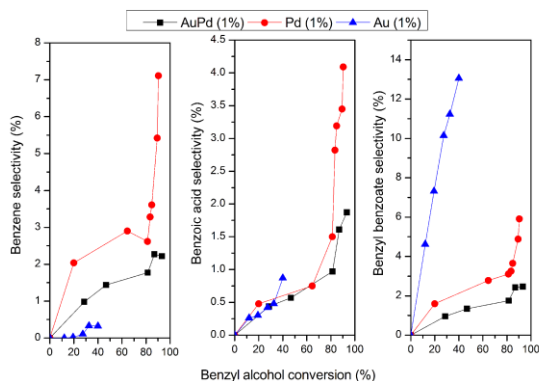


**Figure 4** Selectivity to benzene, benzoic acid and benzyl benzoate as a function of benzyl alcohol conversion over MgAl-  
MMO supported 1% Au-Pd, 1% Pd, and 1% Au

After reaction with benzyl alcohol for 120 min, the catalysts were separated from the reaction mixture by centrifugation, thoroughly washed with acetone, and then reused in the next run under the same conditions. The reusability of the catalysts was investigated for three successive reactions and the results are shown in Figure 5. There was a considerable decrease in catalytic activity over the monometallic Au catalyst during these recycling tests. However, only 6.5% Au leaching is confirmed by ICP

analysis for the deactivated catalyst, indicating that Au leaching is not the sole reason for the activity loss. The deactivation could possibly be due to the aggregation and poisoning of Au nanoparticles. A slight deactivation was also observed in the pure Pd catalyst; however, Pd leaching was observed to be negligible. This indicates that agglomeration and poisoning could also be the main reasons for the deactivation of Pd catalyst. In contrast, the bimetallic Au-Pd catalyst was found to be fully reusable and no metal leaching was observed. In summary, the bimetallic Au-Pd catalyst possessed not only higher activity and benzaldehyde selectivity but also preferable stability during the solvent-free oxidation of benzyl alcohol.

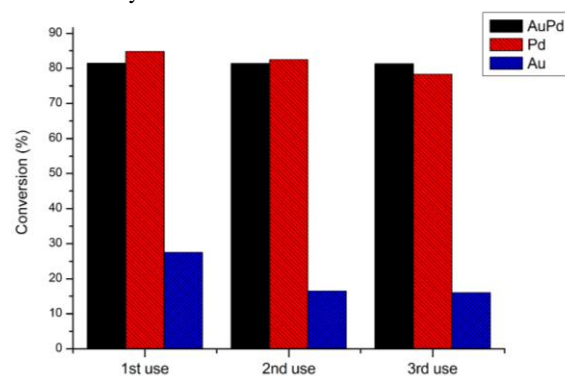


**Figure 5** Reusability of MgAl-  
MMO supported 1% Au-Pd, 1% Pd, and 1% Au

The effect of the Au/Pd molar ratio on activity and selectivity were then investigated and the results are shown in Figure 6. An increase in catalytic activity was observed on increasing the Pd content. This increase of activity reached a maximum with an Au/Pd molar ratio of 1:2. A further increase in the Pd content resulted in a decrease in the catalytic activity. It is important to note that even in the presence of a minor amount of gold or palladium (i.e., in the case of 1:5 and 5:1 Au/Pd molar ratios) an increase in the catalytic activity was observed with respect to the monometallic Au and Pd catalysts. However, by raising the molar fraction of Pd above 0.5, the selectivity to benzaldehyde dropped to 86% for the Au/Pd 1:2 catalyst. Therefore, the optimum selective oxidation of benzyl alcohol to benzaldehyde occurs for the Au/Pd 1:1 molar ratio catalyst with the yield of 87%.

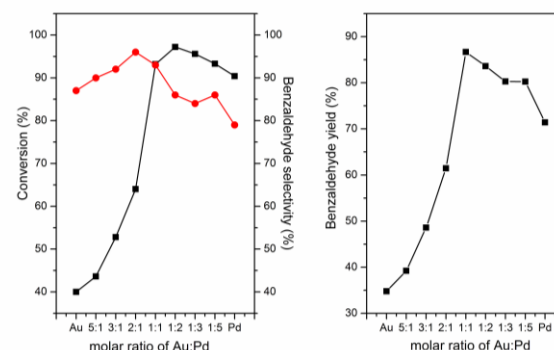


**Figure 6** The effect of Au/Pd molar ratio on the benzyl alcohol conversion (squares), selectivity to benzaldehyde (circles) and yield (Reaction time: 240 min)

## Characterizations of MgAl-MMO supported Au, Pd and Au-Pd catalysts

To investigate the structure of the prepared Au, Pd and Au-Pd nanoparticles, we have initially characterized the colloidal sols with UV-vis spectroscopy and XRD. Figure 7 shows UV-vis spectra of Au, Pd, and Au-Pd bimetallic nanoparticles. The appearance of the plasmon resonance with very weak intensity was observed at about 518 nm which is characteristic for gold nanoparticles with particle sizes below 10 nm.<sup>40</sup> However, as expected there is no surface plasmon band in the Pd sol. The disappearance of the gold surface plasmon band in the spectrum of the bimetallic Au-Pd sol can be attributed to changes in the band structure of the Au nanoparticles due to alloying with Pd. These results suggest the formation of bimetallic nanoalloys, which is in agreement with our previously reported data.<sup>41</sup>

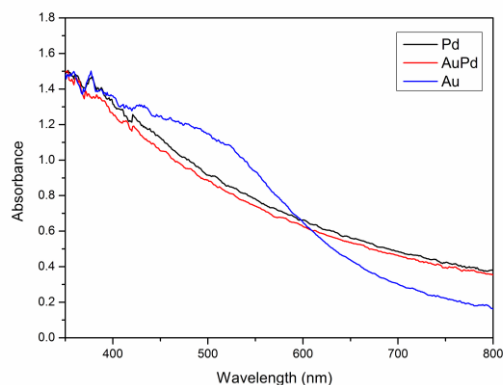


**Figure 7** UV-vis spectra of Au, Pd, and bimetallic Au-Pd nanoparticles

The XRD patterns of Au, Pd, and bimetallic Au-Pd nanoparticles, shown in Figure 8, exhibit two diffraction peaks in the range of  $30^\circ < 2\theta < 70^\circ$  which can be indexed to the (111) and (200) of the fcc structure of monometallic Au and Pd.<sup>42</sup> An obvious shift from pure Au to Pd was observed in the diffraction peaks of the bimetallic Au-Pd particles, indicating the formation of Au-Pd alloys. The  $d_{111}$  and  $d_{200}$  of Pd (0.225 nm and 0.195 nm), Au (0.235 nm and 0.205 nm) and Au-Pd (0.230 nm and 0.200 nm) were calculated according to Bragg formula.

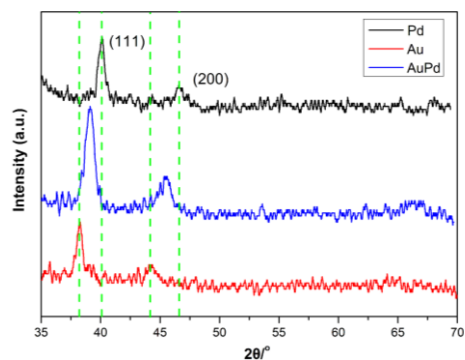


**Figure 8** XRD patterns of Au, Pd and bimetallic AuPd nanoparticles

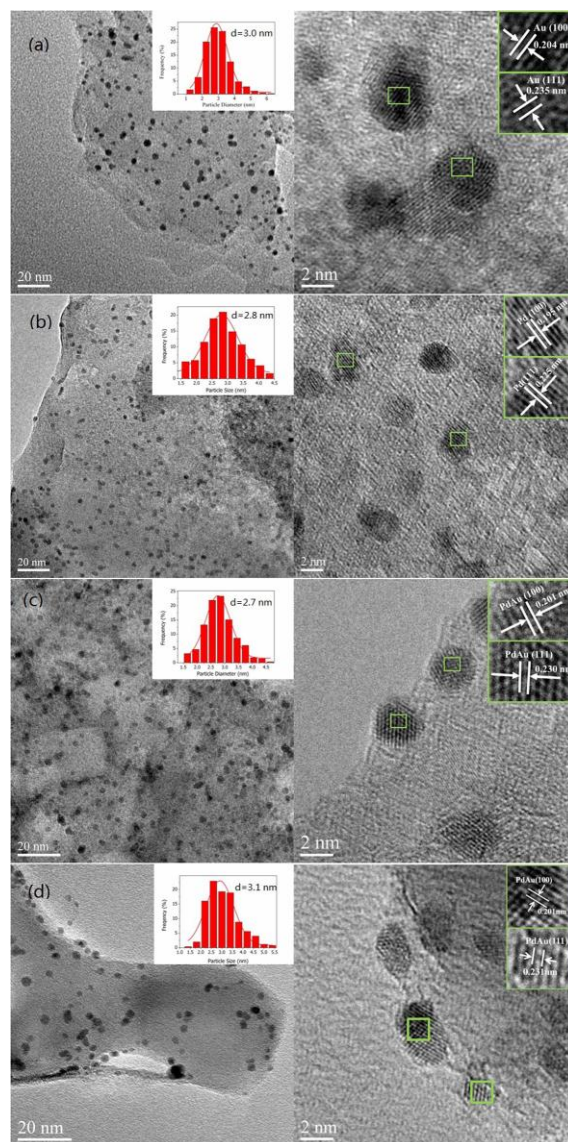


**Figure 9** HRTEM images of 1% Au/MgAl-MMO (a), 1% Pd/MgAl-MMO (b), 1% Au-Pd/MgAl-MMO (c) and 1% Au-Pd/MgO (d)

HRTEM images of the MgAl-MMO supported Au, Pd and bimetallic Au-Pd (Fig. 9 a-c) show that the nanoparticles in all the catalysts are evenly distributed on the surface of MgAl-MMO. The corresponding particle size distributions by measuring more than 200 particles from different regions are also shown. The Au particles cover a wider size distribution and the average size (3.0 nm) is slightly higher than that of Pd (2.8 nm) and Au-Pd (2.7 nm), but these are very similar and there is no visible difference in the morphology of metal nanoparticles. Most of the nanoparticles were cub-octahedra composed of (111) and (100) facets, with the remainder being multiply twinned structures, such as decahedra and icosahedra composed of only (111) facets. The lattice structure of the bimetallic Au-Pd can be observed with 0.230 nm and 0.200 nm of the lattice spacing measured for the adjacent (111) and (100) facet, which are in between the values of Pd (0.225 nm and 0.195 nm) and Au (0.235 nm and 2.04 nm) and

consistent with the XRD results and the values reported in the references.<sup>21,40,43</sup> This change in the lattice constant may lead to both geometric and electronic effects, which in turn might contribute to the interesting chemical properties and enhanced catalytic behaviour we observe. Moreover, no obvious phase contrasts were observed suggesting the absence of core-shell structures, nor were structural incoherencies apparent (assignable to separate monometallic particles) in the bimetallic Au-Pd catalyst, suggesting the absence of segregated monometallic nanoparticles.

IR spectroscopy of CO chemisorption is an excellent method to probe the geometric and electronic structures of bimetallic surfaces.<sup>44,45</sup> Fig. 10 compares IR spectra of CO adsorbed on MgAl-MMO supported Pd, Au and AuPd. It is known that CO adsorbs on Pd in two modes, namely, linear and multi-coordinated; while, CO adsorption onto Au surfaces is weak, and no adsorption band of CO can be generally observed at room temperature. In comparison with the monometallic Pd catalyst, the overall spectral intensity of the bimetallic Au-Pd catalyst decreases significantly. This is because the number of Pd active sites for CO adsorption was reduced due to the alloying of Pd with Au. Moreover, a striking feature in Fig. 10 is that the spectral intensity of a sharp band observed at wavenumbers < 2000  $\text{cm}^{-1}$ , assigned to the multi-coordinated CO species,<sup>46,47</sup> decreases markedly with the addition of Au. The area ratio of linear-bound to multi-bound bands,  $A_l/A_m$ , increased from 0.1 to 0.16, indicating that the addition of Au effectively blocked the sites consisting of two or three adjacent Pd atoms. This trend is in agreement with the literature report that the gold component can separate the contiguous Pd sites in the Au-Pd alloy catalysts until the surface Pd atoms are isolated completely by Au.<sup>18,47,48</sup> According to the presented catalytic data, the single Pd sites, isolated by Au atoms, are suggested to facilitate the coupling of surface species to products while inhibiting the formation of undesirable by-products. This ensemble effect of Au-Pd alloy has also been considered as the origin of unusual reactivity in the reaction of acetylene coupling, selective oxidation of glycerol,  $\text{N}_2\text{O}$  decomposition as well as the direct synthesis of  $\text{H}_2\text{O}_2$ .<sup>42, 49-51</sup> Moreover, it can be seen that the bridged CO on Pd atoms is slightly blue-shifted with the addition of Au, implying there is charge transfer from Pd to Au due to the large electronegativity of Au.<sup>43</sup>

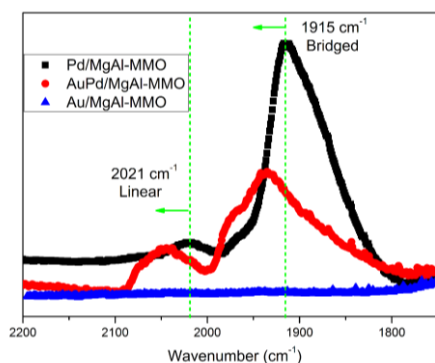


**Figure 10** Transmission FTIR spectra of CO adsorption on monometallic Pd/MgAl-MMO, Au/MgAl-MMO and bimetallic Au-Pd/MgAl-MMO catalyst

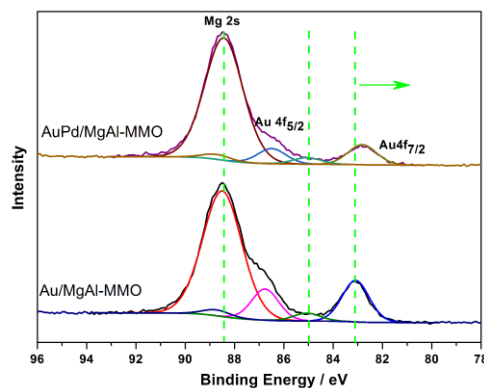


**Figure 11** Au 4f XPS patterns of the pure Au/MgAl-MMO catalyst and bimetallic Au-Pd/MgAl-MMO catalyst

To explore the possibility of electronic interactions between Au and Pd, XPS measurements were performed and the results are shown in Figure 11. Analysis of the Pd is not possible with these low loaded samples as the Pd peaks are obscured by the Mg Auger bands. Therefore, we present only results for the Au 4f signal, although this itself is complicated slightly due to the overlap of the Au 4f<sub>5/2</sub> peak with the Mg 2s photoelectron line. To account for this, we apply a fixed spin orbit splitting of 3.67 eV for the Au 4f doublet, with an area ratio of 4:3 and assume the FWHM of both peaks are equal.

For the Au/MgAl-MMO catalyst, two Au signals are obtained from the results of a perfect fit, at binding energies of 83.1 and 85.0 eV. The binding energy (BE) of the latter species is higher than may be attributed to final state effects alone<sup>52</sup> and therefore this shift is due to a dominance of initial-state effects for a cationic Au<sup>δ+</sup> species and which is likely to be stabilised from bonding to f-centres.<sup>53</sup> The lower BE state is attributed to Au<sup>0</sup>, the low BE a consequence of charge transfer from support to nanoparticle.<sup>54,55</sup> For the bimetallic Au-Pd catalyst, again two gold species are determined from the fitting analysis. However, whilst the Au<sup>δ+</sup> species remains at ca. 85 eV, a distinct shift (0.5 eV) to lower BE for the lower BE Au species was observed. Such shifts suggests that there is charge transfer from Pd to Au as a result of alloy formation and consistent with the results from HRTEM and CO-IR. These synergistic electronic effects in which Au atoms draw electron density away from Pd atoms and thereby increased the catalytic activity.<sup>56</sup>

### Support effect of the Au-Pd catalysts

An understanding of the role of the support may also lead to significant improvements in supported metal catalysts for alcohol oxidation. For this purpose, Au-Pd nanoparticles were immobilized on the commercial MgO as a comparable sample for the Au-Pd/MgAl-MMO catalyst. As shown in Figure 1 and 2, in comparison of MgAl-MMO supported Au-Pd catalyst, the Au-Pd/MgO catalyst exhibited similar selectivity to benzaldehyde, but with much lower benzyl alcohol conversion. After 240 min reaction, the conversion of benzyl alcohol reached only ca. 46%. This confirmed the support is of importance in respect to the

origin of the catalyst activity in benzyl alcohol oxidation as we have noted previously.<sup>13,57</sup> However, both of the pristine MgAl-  
MMO and MgO support are almost inactive in our case. Hence, the benefit of utilizing the MgAl layered mixed oxide as a support  
can be attributed to a cooperative interaction between AuPd nanoparticles and the support surface. Figure 12 shows the XRD  
patterns of the supports and the corresponding catalysts. As expected, the reflections characteristic of a poorly crystalline  
MgO-like phase was observed in the prepared MgAl-  
MMO support which is similar to that reported in the literature for MgAl-  
MMO.<sup>58</sup> However, after immobilisation of metallic nanoparticles, the original reflections of the MgAl-  
MMO have been lost and replaced by the characteristic peaks of an MgAl-  
LDHs phase. This is due to treatment with the solvent during the  
immobilization step LDH layers spontaneously reconstruct their  
original form.<sup>59</sup> During the process of sol immobilisation, the  
MgAl-  
MMO support was dispersed in the aqueous solution for 1  
h, reconstruction of the LDH structure was therefore observed as  
shown by the reappearance of the characteristic (003), (006), (009)  
and (110) reflections.<sup>60</sup> In the case of Au-Pd/MgO catalyst, both  
the characteristic reflections of MgO and Mg(OH)<sub>2</sub> phase were  
observed, indicating a large amount of MgO converted to  
Mg(OH)<sub>2</sub> during the immobilisation of Au-Pd.<sup>61</sup> No XRD  
reflections for Au-Pd species were found in the XRD patterns  
which is due to both small particle sizes and low metal loadings.

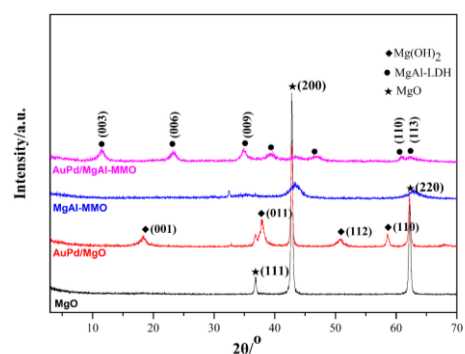


**Figure 12** XRD patterns of the pristine MgAl-  
MMO and MgO support and the supported Au, Pd and Au-Pd catalysts

To gain more insight into differences between the catalysts,  
nitrogen adsorption-desorption measurements were performed to  
shed light on the pore structure of the support. Due to the phase  
transformation of both MgAl-  
MMO and MgO during the sol-  
immobilization process, each support was treated with deionized  
water for the subsequent characterisation. The specific surface  
area of the water treated MgAl-  
MMO support (96 m<sup>2</sup>/g) is much  
higher than that of MgO support (28 m<sup>2</sup>/g) and also MgAl-  
LDH  
precursor (26 m<sup>2</sup>/g). This may have resulted from the formation  
of a large number of shrunk MgAl-  
LDH crystallites during the  
calcination process and the aggregation of the pores in the  
microcrystallites.<sup>58</sup> After complete regeneration of the LDH  
structure during the sol-immobilization process, a large number  
of pores were preserved. As a consequence of the difference in  
specific surface area of MgAl-  
MMO and MgO, AuPd  
nanoparticles are expected to have narrower size distribution and  
therefore smaller average size on the support of MgAl-  
MMO.

HRTEM images and the corresponding size distribution of Au-  
Pd nanoparticles supported on MgO are shown in Fig. 9 (d). In  
contrast to the Au-Pd/MgAl-  
MMO catalyst, the Au-Pd/MgO  
catalyst exhibited a boarder size distribution and slightly larger  
mean size of Au-Pd particles (3.1 nm). Most of smaller particles  
in the Au-Pd/MgO catalyst are cub-octahedral, which are  
consistent with those in the Au-Pd/MgAl-  
MMO catalyst, while the larger particles have an irregular shape. From the high  
magnified image, we can observe that these irregular particles are  
generally composed of two or three Au-Pd alloy cubooctahedra.  
The difference in the size distribution of Au-Pd supported on  
MgAl-  
MMO and MgO can be ascribed to the distinction of their  
surface area. Typically, the fraction of coordinatively unsaturated  
atoms which play dominant roles in the oxidation of benzyl  
alcohol increases with decreasing metal nanoparticle size.<sup>19, 30</sup>  
However, this subtle difference in the size of Au-Pd particles is  
not considered to be the main reason for the disparity in the  
catalytic activity observed for Au-Pd/MgAl-  
MMO and Au-  
Pd/MgO. To investigate the difference between the catalysts, the  
acidity and basicity of the support were determined and the  
results are shown in Figure 13. The CO<sub>2</sub>-TPD profile of the  
MgAl-  
MMO support can be deconvoluted in three main  
desorption peaks, reaching maximum desorption rate at ~233,  
318 °C and 495 °C which can be attributed to the weak, moderate  
and strong basic sites, respectively.<sup>59</sup> The weak and moderate  
basic sites are predominant, representing most contribution of the  
total evolved CO<sub>2</sub>. The peak below 120 °C was assigned to the  
desorption of the physically adsorbed CO<sub>2</sub>. In the case of MgO  
support, the profile also contains three main overlapping peaks;  
while significant shift to higher temperatures were observed,  
illustrating higher basic strengths. The contribution of the strong  
basic sites for MgAl-  
MMO support is much lower than that for  
MgO support, indicating the incorporation of alumina could  
suppress the formation of strong basic sites. Considering the  
relative contributions of the NH<sub>3</sub> desorption peaks (Fig. 13 b), it  
is apparent that the MgAl-  
MMO support possesses at least two  
acidic sites; however, the MgO support, as expected, does not  
possess any acidic sites. The temperature and intensity of the NH<sub>3</sub>  
desorption peak indicates that the MgAl-  
MMO support possesses  
relative strong acidity. In conclusion, the NH<sub>3</sub>-TPD and CO<sub>2</sub>-TPD  
studies reveal that the MgO support has only basic sites, as is to  
be expected; however, the MgAl-  
MMO support possesses both  
acidity and basicity. With the present information on surface  
acidity, it is not possible to assess the type of acid sites and basic  
sites (Bronsted or Lewis), as the TPD cannot distinguish between  
the two. However, these data can aid in determining the origins of  
the catalytic performance.

Based on the significant support effects in the Au-Pd catalyzed  
oxidation of benzyl alcohol we have observed, we suggest that  
acid-base properties of the support play pivotal roles in  
determining both activity and selectivity. The Au-Pd/MgO  
catalyst with stronger basicity but no acidity affords very high  
selectivity to benzaldehyde but quite low activity, whereas the  
Au-Pd/MgAl-  
MMO catalyst with both acidity and basicity  
exhibited not only high activity but also excellent selectivity.  
Therefore, we consider that the acid sites of the support was  
response for the improvement of benzyl alcohol conversion;  
while, the basic sites gave rise to high selectivity to benzaldehyde.

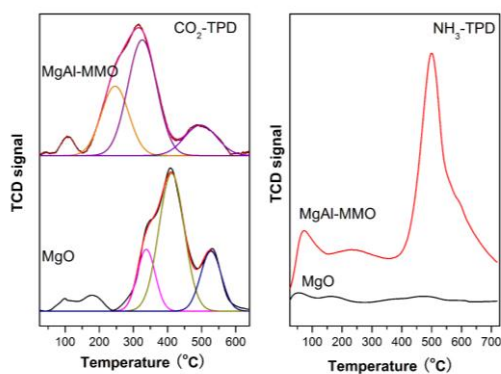


**Figure 13** CO<sub>2</sub> and NH<sub>3</sub>-TPD of deionized water treated MgAl-  
MMO support and MgO support

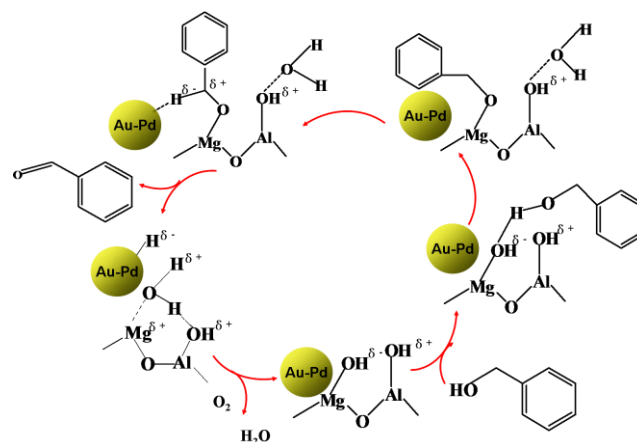
### 5 Mechanism of operation of the bimetallic Au-Pd/MgAl- MMO catalyst

It is generally accepted that the alcohol oxidation over both Pd and Au nanoparticles involves  $\beta$ -H elimination of a dissociated alcohol on the metal surface, which is considered to be the rate-determining step, followed by reaction of oxygen with M-H species.<sup>62-64</sup> The process of  $\beta$ -H elimination is also considered to be the rate-determining step over the bimetallic Au-Pd nanoparticles in our case. The highly improved TON and selectivity to benzaldehyde of the bimetallic Au-Pd catalyst can be attributed to the synergistic effect of Au and Pd. The electronic effects in which Au atoms draw electron density away from Pd atoms enhance the interaction of Pd atoms with the substrate, and thereby increased the catalytic activity; while the geometrical effect in which Au atoms isolated Pd sites inhibited the pathway to the undesired by-products.

In addition to the synergistic effect of Au and Pd, we have demonstrated that the nature of the support also play pivotal roles in the oxidation of benzyl alcohol. On the one hand, the MgAl-LDH support exhibit both basicity and acidity. A base which acts to cleave the O-H bond of the alcohol to form an alkoxide intermediate is often added as a promoter into the catalytic system for aerobic oxidation of alcohols.<sup>65</sup> Therefore, the basic sites on the MgAl-LDH support in our case play a key role in the activation of the O-H bond of the alcohol, to facilitate formation of an adsorbed alkoxide intermediate. While, the acid sites (i.e., AlO-H<sup>δ+</sup>) might participate in the reaction of the metal hydride with oxygen to form water and recover the initial metallic site.<sup>25,30</sup> Simultaneously, AuPd nanoparticles showed a relative narrower size distribution and thus smaller average size on the support of MgAl-  
MMO. The decrease of particle size would increase the amount of coordinatively unsaturated atoms which are also beneficial for the improvement of catalytic activity.

Based on our experimental results and the previous findings,<sup>30,59</sup> we propose a possible mechanism with Au-Pd nanoparticles as active sites (Scheme1), illustrating that the oxidation of benzyl alcohol proceeds through the cooperation between the bimetallic Au-Pd nanoparticles and the base-acid sites on the surface of the MgAl-LDH support. In the first step, benzyl alcohol attacks a basic Mg-OH<sup>δ-</sup> site on the MgAl-LDH,

45 which passes through an abstraction of the proton by the hydroxyl group on the support, to give an alkoxide intermediate at the interface and form a water molecule. We speculate that this step may determine the selectivity, because both Au-Pd/MgAl-  
MMO and Au-Pd/MgO catalyst with basic sites showed very high  
50 selectivity to benzaldehyde. However, the strength of basic sites seems to have little impact on the selectivity. In the second step, the intermediate undergoes coordination to form a metal-H bond with the coordinately unsaturated active centre to afford unsteady metal-alkoholate-LDH species, which undergoes a  $\beta$ -hydride  
55 elimination to give metal-hydride species at the catalyst interface together with the corresponding carbonyl compound. This is expected to be the rate-determining step, and the coordinatively unsaturated metal atoms are more active for the cleavage of this C-H bond. Hence, the catalyst with smaller Au-Pd particles  
60 exhibited higher activity. The third step will be the rapid oxidation of the metal hydride by oxygen to form water promoted by the acid sites of the support while recovering the initial metallic site, thereby completing the catalytic cycle. The proposed mechanism provides fundamental reasons for the higher  
65 activity of Au-Pd nanoparticles on acid-base bifunctional support (MgAl-  
MMO) than on basic MgO.



**Scheme 1** The possible reaction pathway of the solvent free  
70 oxidation for benzyl alcohol over Au-Pd/MgAl-  
MMO catalyst

### Conclusions

We have synthesized a series of MgAl-  
MMO supported Au, Pd and Au-Pd catalysts by a sol-immobilization method and investigated their structural and electronic properties as well as their catalytic behaviour in the solvent-free oxidation of benzyl alcohol with molecular oxygen. Alloying Pd with Au results in an increase of both activity and selectivity to benzaldehyde and, moreover, an improved resistance to catalyst deactivation  
80 compared with the monometallic Pd and Au catalysts. The TON over the Au/Pd 1:1 molar ratio catalyst achieved 13000 after 240 min and the selectivity to benzaldehyde was maintained at 93% throughout and the catalysts are fully reusable. XRD, UV-vis and HRTEM confirmed the formation of Au-Pd nanoalloys with the  
85 average size of 2.7 nm instead of core-shell bimetallic particles and segregated monometallic particles. The ensemble and electronic effect between Pd and Au in the Au-Pd/MgAl-  
MMO

catalyst were revealed by IR spectroscopy of CO chemisorption and XPS analysis. The electronic effects in which Au atoms draw electron density away from Pd atoms enhanced the interaction of Pd atoms with the substrate, and thereby increased the catalytic activity. While, the geometrical effect in which Au atoms isolated Pd sites inhibited the pathway to the undesired by-products.

In order to investigate the support effect, Au-Pd/MgO catalyst was prepared for comparison. The promotional effect of the MgAl-MMO support on the catalytic activity for benzyl alcohol oxidation suggested that the acid sites of the support was response for the improvement of catalytic activity; while, the basic sites gave rise to high selectivity. A possible mechanism with Au-Pd nanoparticles as active sites was proposed, illustrating that the oxidation of benzyl alcohol would proceed through the cooperation between the Au-Pd nanoalloys and the base/acid sites on the surface of the support.

## Acknowledgments

The work was financially supported by the 973 Project of China (2011CBA00506), the Support Plan Project of China (2012BAE06B08), the Natural Science Foundation of Beijing (2132032) and China Scholarship Council. We also thank Cardiff University for financial support.

## References

- 1 S. E. Davis, M. S. Ide and R. J. Davis, *Green Chem.*, 2013, **15**, 17.
- 2 R. Ferrando, J. Jellinek and R. L. Johnston, *Chem. Rev.*, 2008, **108**, 847.
- 3 D. S. Wang and Y. D. Li, *Adv. Mater.*, 2011, **23**, 1044.
- 4 M. Sankar, N. Dimitratos, P. J. Miedziak, P. P. Wells, C. J. Kiely and G. J. Hutchings, *Chem. Soc. Rev.*, 2012, **41**, 8099.
- 5 M. Contea, A. F. Carley, G. Attarda, A. A. Herzing, C. J. Kiely and G. J. Hutchings, *J. Catal.*, 2008, **257**, 190.
- 6 F. Ye, H. Liu, W. W. Hu, J. Y. Zhong, Y. Y. Chen, H. B. Cao and J. Yang, *Dalton Trans.*, 2012, **41**, 2898.
- 7 G. L. Brett, Q. He, C. Hammond, P. J. Miedziak, N. Dimitratos, M. Sankar, A. A. Herzing, M. Conte, J. A. Lopez-Sanchez, C. J. Kiely, D. W. Knight, S. H. Taylor, and G. J. Hutchings, *Angew. Chem.*, 2011, **123**, 10318.
- 8 G. ten Brink, I. W. C. E. Arends and R. A. Sheldon, *Science*, 2000, **287**, 1636.
- 9 A. Abad, P. Concepcin, A. Corma and H. García, *Angew. Chem. Int. Ed.*, 2005, **44**, 4066.
- 10 N. Dimitratos, J. A. Lopez-Sanchez, D. Morgan, A. F. Carley, R. Tiruvalam, C. J. Kiely, D. Bethell and G. J. Hutchings, *Phys. Chem. Chem. Phys.*, 2009, **11**, 5142.
- 11 P. J. Miedziak, Q. He, J. K. Edwards, S. H. Taylor, D. W. Knight, B. Tarbit, C. J. Kiely and G. J. Hutchings, *Catal. Today*, 2011, **163**, 47.
- 12 M. Pagliaro, S. Campestrini and R. Ciriminna, *Chem. Soc. Rev.*, 2005, **34**, 837.
- 13 M. Sankar, E. Nowicka, R. Tiruvalam, Q. He, S. H. Taylor, C. J. Kiely, D. Bethell, D. W. Knight and G. J. Hutchings, *Chem. Eur. J.*, 2011, **17**, 6524.
- 14 A. Abad, P. Concepcin, A. Corma, and H. García, *Angew. Chem. Int. Ed.*, 2005, **44**, 4066.
- 15 F. Z. Su, Y. M. Liu, L. C. Wang, Y. Cao, H. Y. He and K. N. Fan, *Angew. Chem. Int. Ed.*, 2008, **120**, 340.
- 16 C. Della Pina, E. Falletta, M. Rossi, *J. Catal.*, 2008, **260**, 384.
- 17 A. S. K. Hashmi and G. J. Hutchings, *Angew. Chem. Int. Ed.*, 2006, **45**, 7896.
- 18 D. I. Enache, J. K. Edwards, P. Landon, B. Solsona-Espriu, A. F. Carley, A. A. Herzing, M. Watanabe, C. J. Kiely, D. W. Knight and G. J. Hutchings, *Science*, 2006, **311**, 362.
- 19 L. Kesavan, R. Tiruvalam, M. H. Ab Rahim, M. I. bin Saiman, D. I. Enache, R. L. Jenkins, N. Dimitratos, J. A. Lopez-Sanchez, S. H. Taylor, D. W. Knight, C. J. Kiely and G. J. Hutchings, *Science*, 2011, **311**, 195.
- 20 J. Pritchard, L. Kesavan, M. Piccinini, Q. He, R. Tiruvalam, N. Dimitratos, J. A. Lopez-Sanchez, A. F. Carley, J. K. Edwards, C. J. Kiely and G. J. Hutchings, *Langmuir*, 2010, **26**, 16568.
- 21 N. Dimitratos, A. Villa, D. Wang, F. Porta, D. S. Su and L. Prati, *J. Catal.*, 2006, **244**, 113.
- 22 D. Wang, A. Villa, P. Spontoni, D. S. Su and L. Prati, *Chem. Eur. J.*, 2010, **16**, 10007.
- 23 Z. Yin, M. F. Chi, Q. J. Zhu, D. Ma, J. M. Sun and X. H. Bao, *J. Mater. Chem. A*, 2013, **1**, 9157.
- 24 A. Villa, D. Wang, N. Dimitratos, D. S. Su, V. Trevisan and L. Prati, *Catal. Today*, 2010, **150**, 8.
- 25 S. J. Mejía-Rosales, C. Fernández-Navarro, E. Pérez-Tijerina, D. A. Blom, L. F. Allard and M. José-Yacamán, *J. Phys. Chem. C* 2007, **111**, 1256.
- 26 K. Shimizu, K. Sugino, K. Sawabe and A. Satsuma, *Chem. Eur. J.*, 2009, **15**, 2341.
- 27 J. Chen, Q. Zhang, Y. Wang and H. Wan, *Adv. Synth. Catal.* 2008, **350**, 453.
- 28 A. Villa, C. E. Chan-Thaw, G. M. Veith, K. L. More and D. Ferri, L. Prati, *Chem. Cat. Chem.*, 2011, **3**, 1612.
- 29 H. Sun, F. Z. Su, J. Ni, Y. Cao, H. Y. He and K. N. Fan, *Angew. Chem. Int. Ed.*, 2009, **48**, 4390.
- 30 W. Fang, J. Chen, Q. Zhang, W. Deng and Y. Wang, *Chem. Eur. J.*, 2011, **17**, 1247.
- 31 D. I. Enache, D. W. Knight and G. J. Hutchings, *Catal. Lett.*, 2005, **103**, 43.
- 32 M. Sankar, E. Nowicka, R. Tiruvalam, Q. He, S. H. Taylor, C. J. Kiely, D. Bethell, D. W. Knight and G. J. Hutchings, *Chem. Eur. J.*, 2011, **17**, 6524.
- 33 D. G. Evans, R.C.T. Slade, *Struct. Bond.*, 2006, **119**, 1.
- 34 J. T. Feng, Y. J. Lin, D. G. Evans, X. Duan, D. Q. Li, *J. Catal.*, 2009, **266**, 351.
- 35 L. He, Y. Q. Huang, A. Q. Wang, Y. Liu, X. Y. Liu, X. W. Chen, J. José Delgado, X. D. Wang and T. Zhang, *J. Catal.*, 2013, **298**, 1.
- 36 B. M. Choudary, S. Madhi, N. S. Chowdari, M. L. Kantam and B. Sreedhar, *J. Am. Chem. Soc.*, 2002, **124**, 14127.
- 37 X. D. Lei, F. Z. Zhang, L. Yang, X. X. Guo, Y. Y. Tian, S. S. Fu, F. Li, D. G. Evans and X. Duan, *AIChE J.*, 2007, **53**, 932.
- 38 B. R. Strohmeier, *Surf. Sci. Spectra*, 1994, **2**, 121.
- 39 D. I. Enache, D. Barker, J. K. Edwards, S. H. Taylor, D. W. Knight, A. F. Carley and G. J. Hutchings, *Catal. Today*, 2007, **122**, 407.
- 40 R. J. Nikhil, G. Latha, and M. Catherine J., *Langmuir*, 2001, **17**, 6783.
- 41 J. A. Lopez-Sanchez, N. Dimitratos, P. Miedziak, E. Ntainjua, J. K. Edwards, D. Morgan, A. F. Carley, R. Tiruvalam, C. J. Kiely and G. J. Hutchings, *Phys. Chem. Chem. Phys.*, 2008, **10**, 1921.
- 42 Y. W. Lee, N. H. Kim, K. Y. Lee, K. Kwon, M. Kim and S. W. Han, *J. Phys. Chem. C*, 2008, **112**, 6717.
- 43 X. Wei, X. F. Yang, A. Q. Wang, L. Li, X. Y. Liu, T. Zhang, C. Y. Mou and J. Li, *J. Phys. Chem. C*, 2012, **116**, 6222.
- 44 F. Gao, Y. L. Wang and D. W. Goodman, *J. Am. Chem. Soc.*, 2009, **131**, 5734.
- 45 N. Toshima and T. Yonezawa, *New J. Chem.*, 1998, **22**, 1179.
- 46 J. Rebelli, M. Detwiler, S. Ma, C. T. Williams and J. R. Monnier, *J. Catal.*, 2010, **270**, 224.
- 47 H. L. Abbott, A. Aumer, Y. Lei, C. Asokan, R. J. Meyer, M. Sterrer, S. Shaikhutdinov and H.-J. Freund, *J. Phys. Chem. C*, 2010, **114**, 17099.
- 48 M. S. v. Chen, D. Kumar, C. W. Yi and D. W. Goodman, *Science*, 2005, **310**, 291.
- 49 A. F. Lee, C. J. Baddeley, C. Hardacre, R. M. Ormerod, R. M. Lambert, G. Schmid and H. J. West, *Phys. Chem.*, 1995, **99**, 6096.
- 50 D. Wang, A. Villa, F. Porta, L. Prati and D. S. Su, *J. Phys. Chem. C*, 2008, **112**, 8617.
- 51 H. C. Ham, G. S. Hwang, J. Han, S. W. Nam and T. H. Lim, *J. Phys. Chem. C*, 2009, **113**, 12943.
- 52 M. Baron, O. Bondarchuk, D. Stacchiola, S. K. Shaikhutdinov and H.-J. Freund, *J. Phys. Chem. C*, 2009, **113**, 6042.

- 53 R. P. Socha, E. Zackiewicz, N. Spiridis and J. Korecki, *Surf. Interface Anal.*, 2010, **42**, 536.
- 54 M. Murdoch, G. I. N. Waterhouse, M. A. Nadeem, J. B. Metson, M. A. Keane, R. F. Howe, J. Llorca and H. Idriss, *Nature Chem.*, 2011, **3**, 489.
- 55 S. Arrii, F. Morfin, A. J. Renouprez and J. L. Rousset, *J. Am. Chem. Soc.*, 2004, **126**, 1199.
- 56 W. Hou, N. A. Dehm and R. W.J. Scott, *J. Catal.*, 2008, **253**, 22.
- 57 M. Sankar, E. Nowicka, P. J. Miedziak, G. L. Brett, R. L. Jenkins, N. Dimitratos, S. H. Taylor, D. W. Knight, D. Bethell and G. J. Hutchings, *Faraday Discuss.*, 2010, **145**, 341.
- 58 X. D. Lei, W. Lu, Q. Peng, H. Y. Li, T. Chen, S. L. Xu and F. Z. Zhang, *Appl. Catal. A: Gen.*, 2011, **399**, 87.
- 59 T. Chen, F. Z. Zhang and Y. Zhu, *Catal. Lett.*, 2013, 143, 206.
- 60 J. T. Feng, X. Y. Ma, Y. F. He, D. G. Evans and D. Q. Li, *Appl. Catal. A: Gen.*, 2012, **10-20**, 413.
- 61 R. Giorgi, C. Bozzi, L. Dei, C. Gabbiani, B. W. Ninham and P. Baglioni, *Langmuir*, 2005, **21**, 8495.
- 62 M. Conte, H. Miyamura, S. Kobayashi and V. Chechik, *J. Am. Chem. Soc.*, 2009, **131**, 7189.
- 63 Hi. Tsunoyama, H. Sakurai, Y. Negishi and T. Tsukuda, *J. Am. Chem. Soc.*, 2005, **127**, 9374.
- 64 A. Abad, A. Corma and H. García, *Chem. Eur. J.*, 2008, **14**, 212.
- 65 T. Ishida, M. Nagaoka and T. Akita, M. Haruta, *Chem. Eur. J.*, 2008, **14**, 8456.

25